Supporting Information

Alloying and interface effects endow supported-PtRuCo nanochains 70,000-cycle stability in neutral hydrogen evolution

Yangqin Feng and Qiang Yuan*

State Key Laboratory of Green Pesticide, Center for R&D of Fine Chemicals, College of Chemistry and Chemical Engineering, Guizhou University, Guiyang, Guizhou Province 550025, PR China.

* Corresponding author

E-mail address: qyuan@gzu.edu.cn

This PDF file includes
Supplementary Characterization
Supplementary Figure S1-S31
Supplementary Table S1-S5

Experimental Section

Chemicals:

Chloroplatinic (IV) acid hexahydrate ($H_2PtCl_6 \cdot 6H_2O$, 99%) was purchased from CIVI-CHEM. Ruthenium (III) chloride hydrate ($RuCl_3 \cdot xH_2O$, 99.9%) was purchased from Aldrich. Hexadecyltrimethylammonium bromide ($(C_{19}H_{42}BrN)$, CTAB, AR), Dopamine hydrochloride ($C_8H_{12}ClNO_2$, 98%) and Cobalt chloride hexahydrate ($CoCl_2 \cdot 6H_2O$, 99.9%) were purchased from Aladdin. Ammonium molybdate tetrahydrate ($(NH_4)_6Mo_7O_{24} \cdot 4H_2O$, 99.9%) and Potassium hydroxide (KOH, 95%) were purchased from Macklin. Ammonium hydroxide ($NH_3 \cdot H_2O$, 25~28%), Sulfuric acid (H_2SO_4, 98%), Ethylene glycol (EG, 99%, AR), Ethanol (AR), Potassium phosphate monobasic (KH_2PO_4, 99%) and Disodium hydrogen phosphate dodecahydrate ($Na_2HPO_4 \cdot 12H_2O$, 99%) were purchased from Sinopharm Chemical Reagent Co. Ltd. (Shanghai, China). 20% Pt/C was purchased from Johnson Matthey. 20% Ru/C was obtained from Premetek. Commercial IrO_2 was obtained from Alfa-Aesar. All chemicals were used without further purification.

Synthesis of hollow Mo_2C nanoflowers:

The synthesis of hollow molybdenum carbide nanoflowers was slightly adapted from previously published work [1]. In brief, 370 mg $(NH_4)_6Mo_7O_{24} \cdot 4H_2O$ was added into a bottle containing 30 mL of deionized water and stirred magnetically to obtain a uniform solution. Then 200 mg $C_8H_{12}ClNO_2$ was added and stirred for 20 min to obtain a clear red solution. After adding 60 mL of ethanol and stirring for 5 min, 0.25 mL of $NH_3 \cdot H_2O$ was added quickly to adjust the pH value and stir for 3 h at room temperature. The orange-red products were collected by centrifugation and washed with ethanol several times (10000 rpm for 15 min), then dried under vacuum at 60 °C overnight (called hollow Mo-PDA). Finally, the hollow Mo-PDA precursor was calcined in a tube furnace at 800 °C under an argon atmosphere for 2 h to obtain a black powder.

Synthesis of PtRuCo/Mo_2C:

Typically, aqueous solutions of H_2PtCl_6 (0.15 mL; 0.1 M), $RuCl_3$ (0.125 mL; 0.1 M) and $CoCl_2$ (0.125 mL; 0.1 M), 36.4 mg CTAB, 15 mg Mo_2C powder were added in 10 mL of deionized water and 10 mL of ethylene glycol in 50 mL Teflon-lined stainless-steel autoclave. After sonication for 10 min and stirring for 1-2 min, 0.25 mL of $NH_3 \cdot H_2O$ was added and stirred for 60 min. Then the sealed vessel was heated at 180 °C for 6 h. After cooling down to room temperature, the black catalysts were washed with ethanol and centrifuged several times (10000 rpm for 15 min). Finally, the final products were dispersed in 8 mL of ethanol. Pt/Mo_2C, PtRu/Mo_2C, PtCo/Mo_2C, and pure PtRuCo in the same way without the addition of Pt, Ru, Co and Mo_2C. The molar ratios of 6:6:6, 5:5:5,

and 4:5:5 of Pt: Ru: Co were synthesized using the same method, respectively.

Characterization

The morphology of samples was analyzed by transmission electron microscopy (TEM; JEM-1400 Flash at 120 KV, JEOL), scanning electron microscope (SEM; Apreo 2C, Thermo Fisher Scientific), and double spherical aberration-corrected (AC) high-resolution TEM (AC-HRTEM; FEI, Themis Z). The X-ray diffraction (XRD) spectrum of the samples was recorded on a Bruker D8 ADVANCE X-ray powder diffractometer with Cu Kα radiation (λ = 1.5418 Å) and graphite monochromator (40 KV, 40 mA). X-ray photoelectron spectroscopy (XPS) measurements were performed using a PHI VersaProbe 4 Scanning XPS Microprobe (ULVAC-PHI Inc.) using Al Kα X-ray radiation (1486.6 eV) for excitation. The binding energy was corrected from charge effects by reference to the C 1s peak of carbon at 284.8 eV. Inductively Coupled Plasma Optical Emission Spectrometry (ICP-OES; iCAP 7200, Thermo Fisher Scientific) was used to analyze the elemental content of the samples. In situ Raman measurements were carried out on LabRAM HR Evolution spectrometer (Horida Scientific) with an excitation wavelength of 532 nm. In-situ attenuated total reflectance surface-enhanced infrared absorption spectroscopy (ATR-SEIRAS) were collected on Nicolet iS50 spectrometer (Thermo Fisher Scientific).

Electrochemical measurements

The electrochemical measurements were performed on a CHI 760E (CH Instruments, Shanghai) workstation using a typical three-electrode cell saturated with nitrogen at room temperature. The working electrode was the glassy carbon rotating-disk electrode (diameter: 5 mm, area: 0.196 cm^2, PINE company, USA). A graphite rod was used as the counter electrode, and Hg/HgO (1.0 M KOH) or Ag/AgCl (0.5 M H_2SO_4, 1.0 M PBS) electrodes served as the reference electrodes.

Preparation of sample ink: The as-prepared electrocatalysts (5 mg) were first dispersed in a mixed solvent containing 800 μL of ethanol and 200 μL of 0.1% Nafion solution via ultrasonication for another 30 min. The GC electrode was polished with 50 nm polishing powder, ultrasonically cleaned with deionized water and ethanol, and dried before use. Then, the as-prepared catalyst ink was dropped onto the GC electrode to obtain the working electrode, and the loading amount of the precious metal (Pt, Ru or Pt+Ru) for all samples was ~10.2 μg/cm^2.

The linear sweep voltammetry (LSV) curves of all the samples were obtained at a scan rate of 10 mV/s, with iR compensation at 1,600 rpm. The Electrochemical impedance spectroscopy (EIS) tests

were performed in the frequency range of 100 kHz-0.01 Hz with an amplitude of 10 mV.

For stability testing, the catalyst was evaluated using the continuous CV method from -0.1 V to 0.1 V (versus RHE) at a scan rate of 100 mV s^{-1} for 10,000 cycles.

For long term stability test, the $Pt_{0.5}Ru_{0.22}Co_{0.28}/Mo_2C$ catalyst was tested under the ISTEP - Multi-Current Steps mode (@ 10, 20, 25, 50 mA cm^{-2} for 10 hours at each current density, totally for 80 h).

All the measured potentials were converted to the reversible hydrogen electrode (RHE) using the following equations:

$E_{RHE} = E_{Hg/HgO} + 0.098\ V + 0.059 \times pH$ (in 1.0 M KOH)

$E_{RHE} = E_{Ag/AgCl} + 0.197\ V + 0.059 \times pH$ (in 0.5 M H_2SO_4 or 1.0 M PBS)

The electrochemically active surface area (ECSA) of the electrocatalyst was calculated using the following formula:

$$ECSA = \frac{CDL}{C_S}$$

$CDL = C_{dl} \times 0.196\ cm^2$, $C_S = 0.04\ mF\ cm^{-2}$

To calculate the double-layer capacitance (C_{dl}) of these electrocatalysts, cyclic voltammetry (CV) curves were obtained at different scan rates (10, 15, 20, 30, 40, 50 mV/s) in the non-Faradaic potential region of the electrocatalyst in 1.0 M PBS solution.

The Tafel slopes (b) were extracted from the LSV curves and used to evaluate the HER kinetics of the electrocatalysts by fitting the linear segment to the Tafel equation:

$\eta = b \log(j) + a$

where η represents the overpotential, j means the current density, and a is the Tafel constant.

The mass activity (MA) of the catalyst can be calculated by this formula:

$$j_{mass} = \frac{j\ (A\ cm^{-2})}{mass_{PGM}\ (mg\ cm^{-2})}$$

The TOF value can be calculated using the following equation [2]:

$$TOF(H_2/s) = \frac{|j| \cdot A}{m \cdot F \cdot n(total)}$$

where |j| represents the current density (mA cm^{-2}), A means the electrode geometric area (cm^2), m stands for the number of electrons per H_2 (m = 2 for HER), F represents the Faraday constant

(96485 C mol^{-1}), and n (total) denotes the molar amount of active sites specific to the target species.

In-situ Raman measurements

The Raman spectra were collected on LabRAM HR Evolution (532 nm laser). The in-situ Raman spectrum was performed in a Raman cell with PtRuCo/Mo_2C decorated GC electrode as the working electrode, the Pt wire as the counter electrode, and the Ag/AgCl (saturated KCl) as the reference electrode, respectively, in 1.0 M PBS solution. The potential range was set from -0.3 to -0.8 V vs. Ag/AgCl.

In-situ ATR-SEIRAS measurements

The in-situ ATR-SEIRAS measurements were performed on Nicolet iS50 spectrometer. The electrochemical experiments were conducted in a three-electrode cell with 0.1 M PBS as the electrolyte. The gold film loaded with catalyst served as the working electrode, a graphite rod as the counter electrode and the Ag/AgCl (saturated KCl) as the reference electrode, respectively. The potential range during the measurements was set from 0 V to -1.0 V versus RHE.

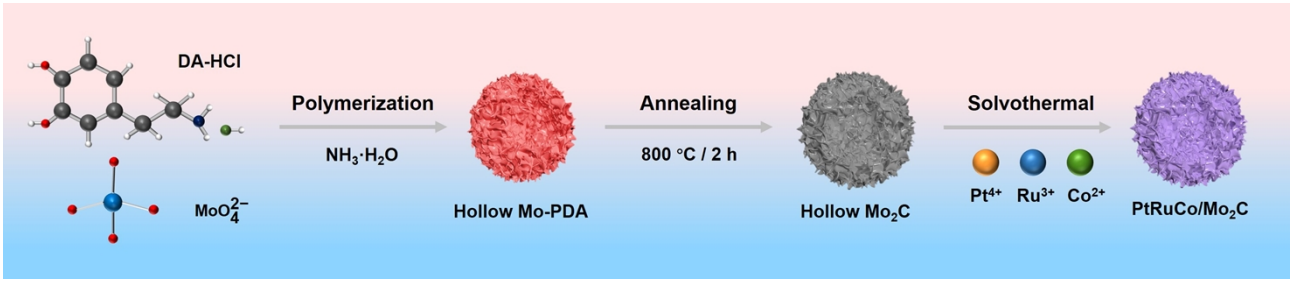

Figure S1. (a) Schematic illustration of the synthesis of PtRuCo/Mo_2C.

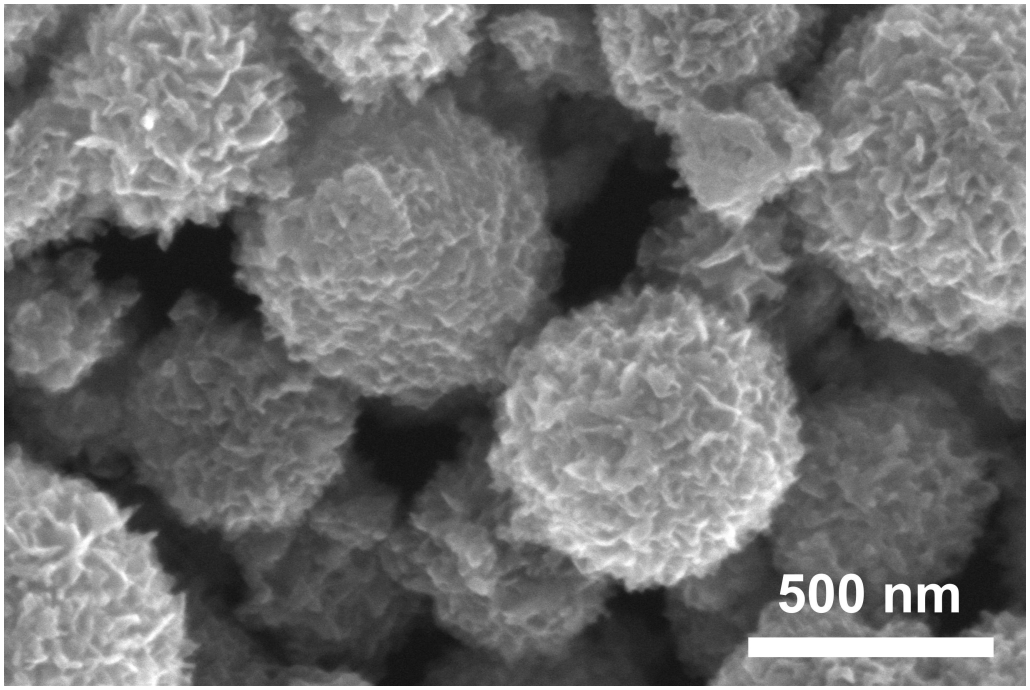

Figure S2. Scanning electron microscopy (SEM) image of Hollow Mo_2C.

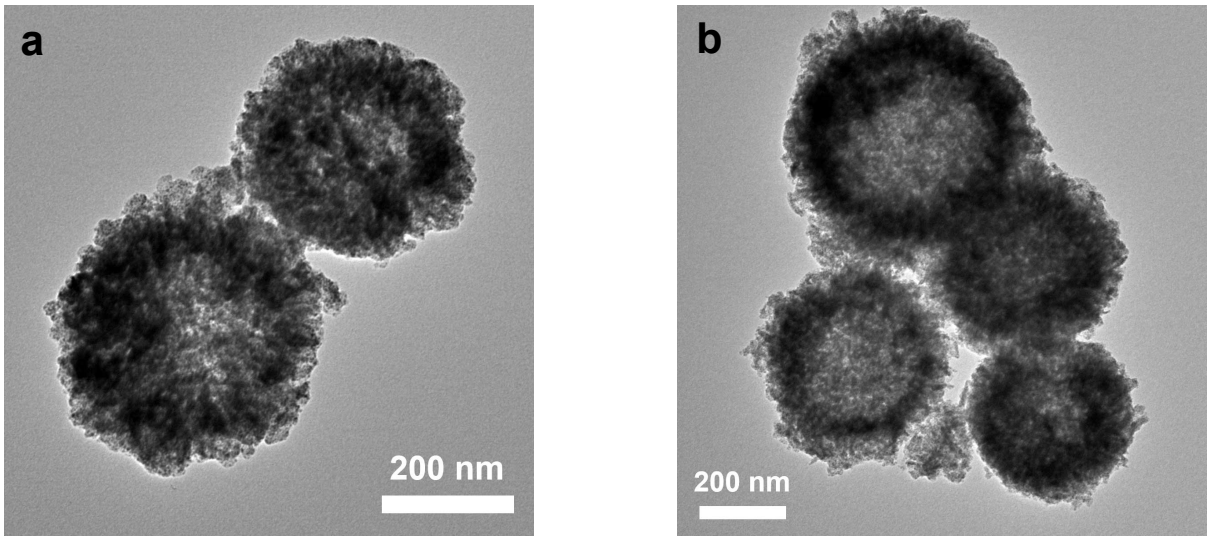

Figure S3. Transmission electron microscopy (TEM) images of hollow Mo_2C.

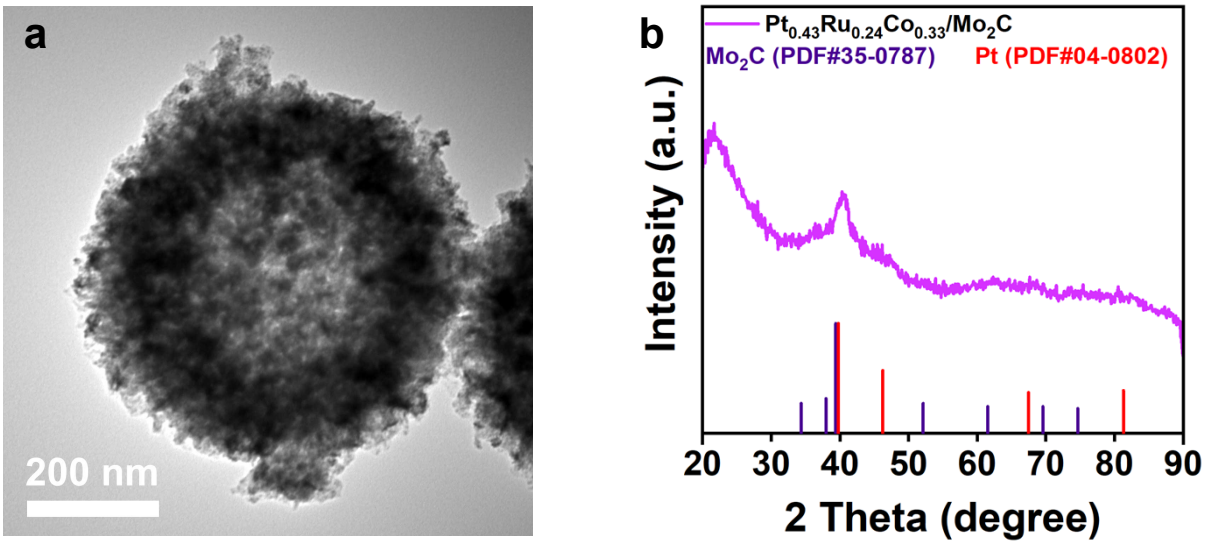

Figure S4. (a) TEM image and (b) XRD pattern of $Pt_{0.43}Ru_{0.24}Co_{0.33}/Mo_2C$.

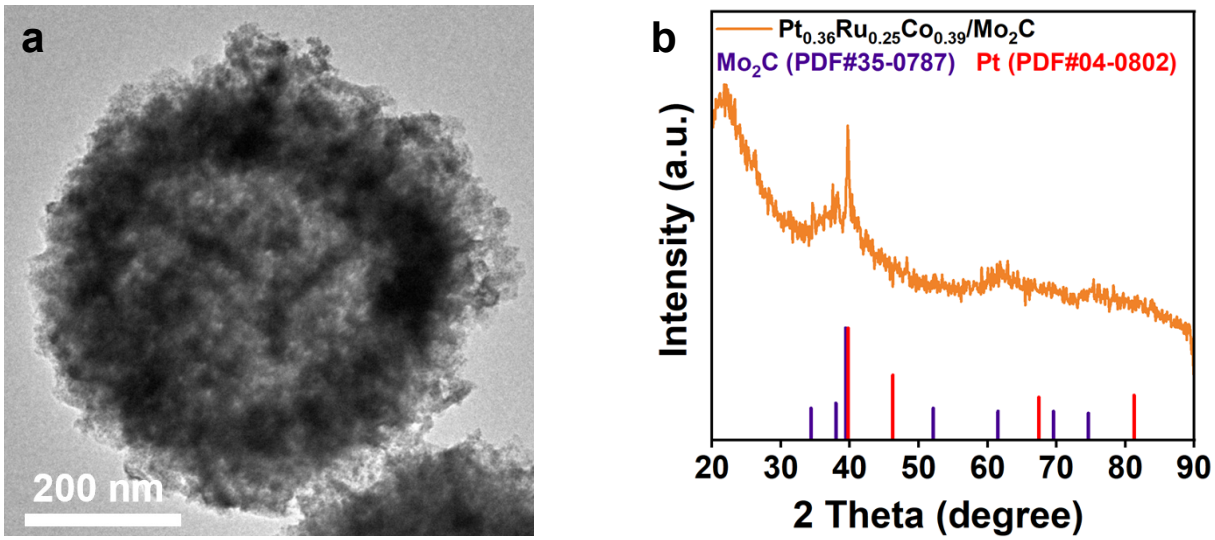

Figure S5. (a) TEM image and (b) XRD pattern of $Pt_{0.36}Ru_{0.25}Co_{0.39}/Mo_2C$.

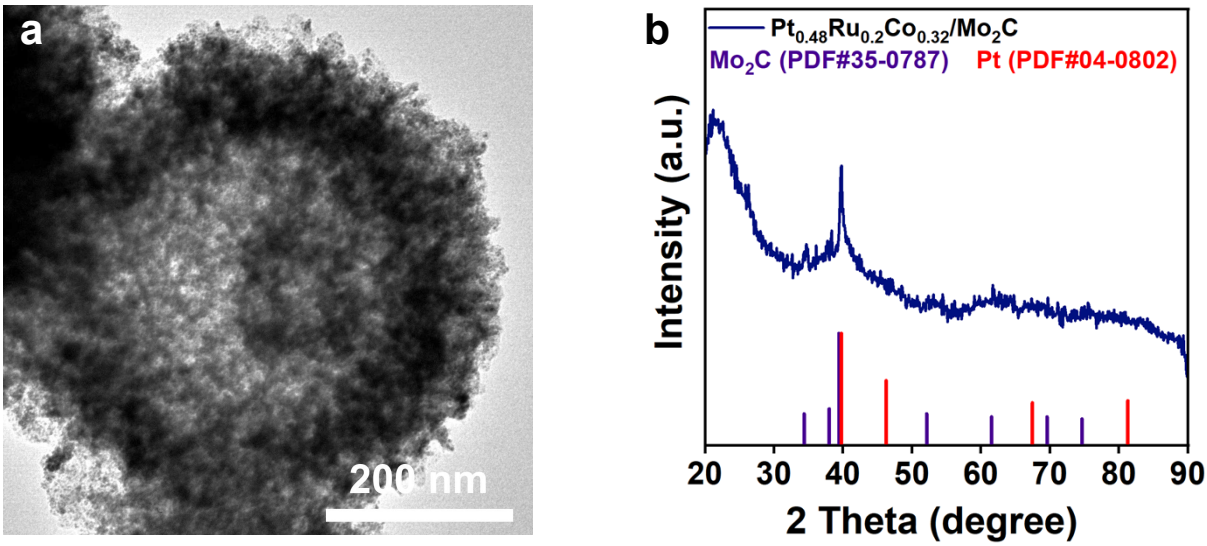

Figure S6. (a) TEM image and (b) XRD pattern of $Pt_{0.48}Ru_{0.2}Co_{0.32}/Mo_2C$.

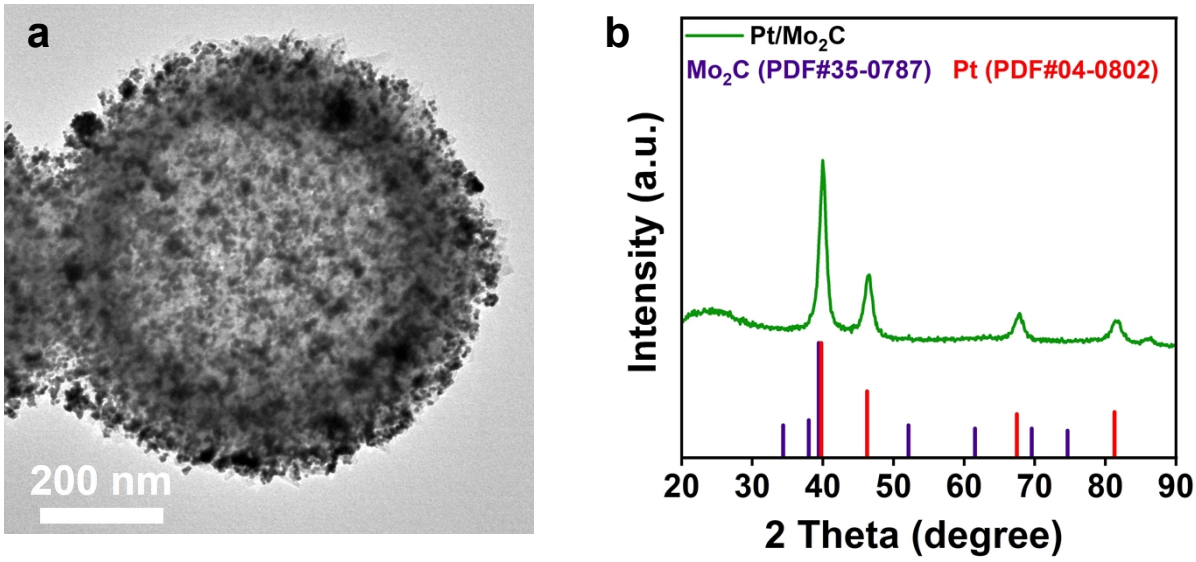

Figure S7. (a) TEM image and XRD pattern of Pt/Mo_2C.

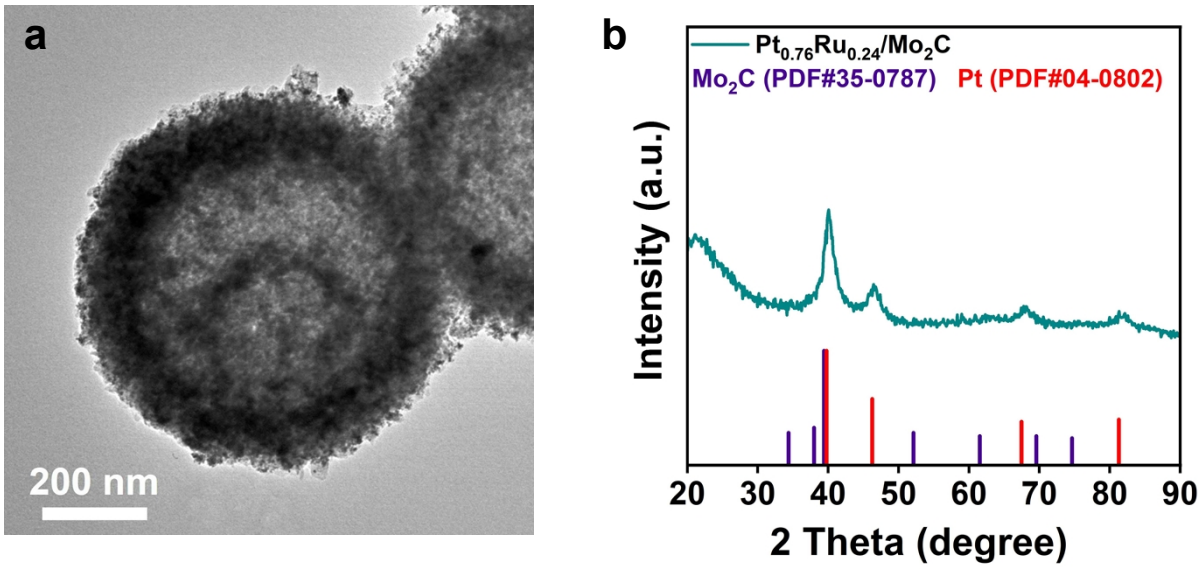

Figure S8. (a) TEM image and XRD pattern of $Pt_{0.76}Ru_{0.24}/Mo_2C$.

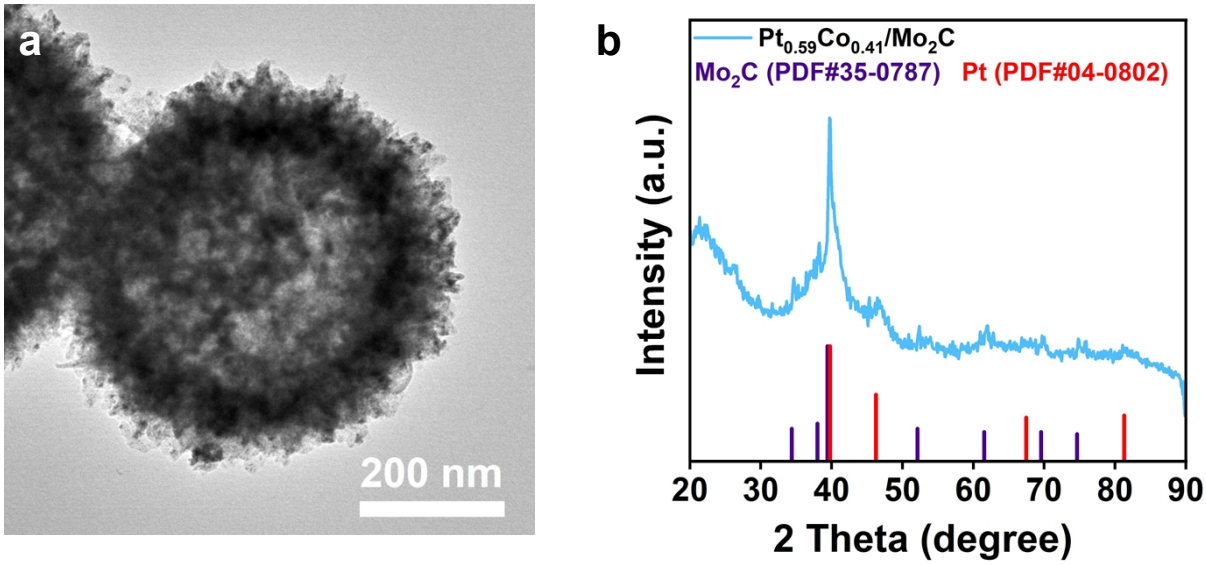

Figure S9. (a) TEM image and XRD pattern of $Pt_{0.59}Co_{0.41}/Mo_2C$.

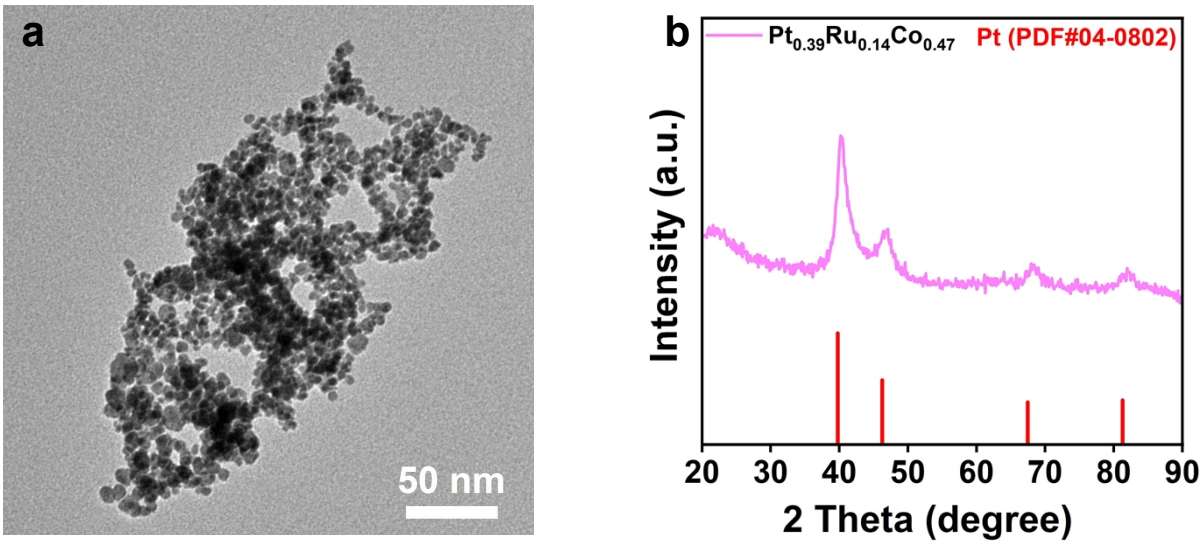

Figure S10. (a) TEM image and XRD pattern of $Pt_{0.39}Ru_{0.14}Co_{0.47}$.

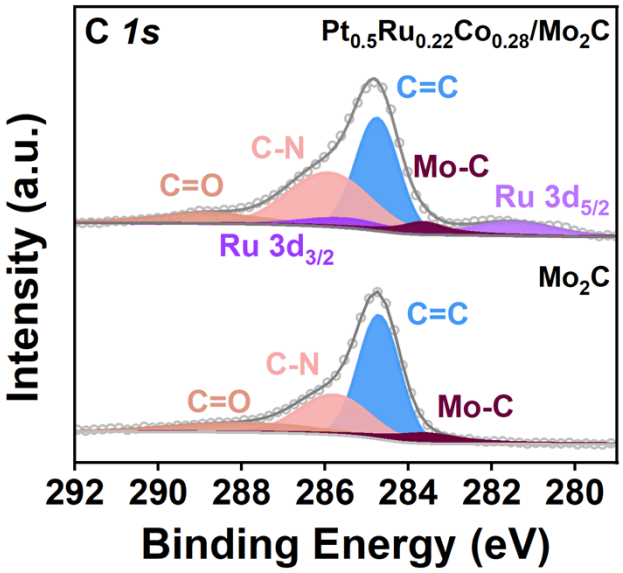

Figure S11. C 1s high-resolution XPS spectra.

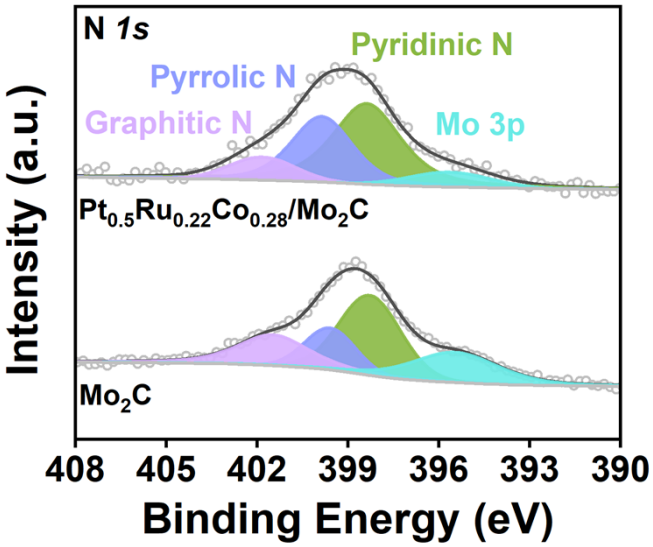

Figure S12. N 1s high-resolution XPS spectra.

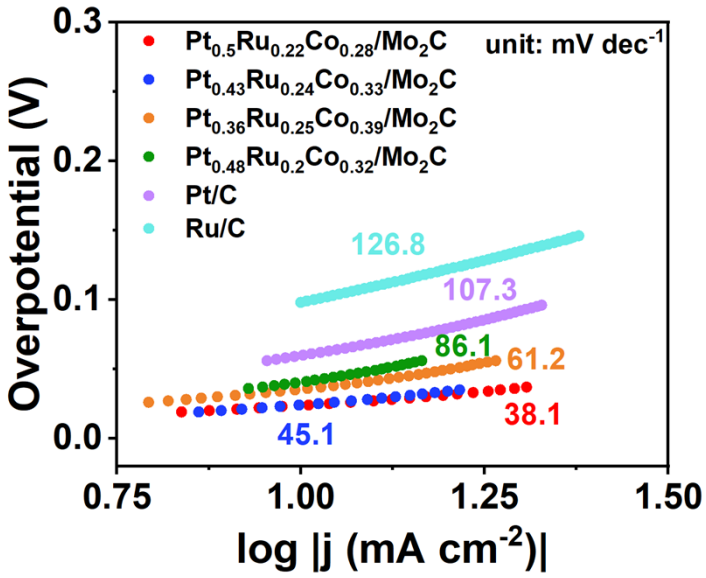

Figure S13. Tafel plots of PtRuCo/Mo_2C series catalysts, Pt/C and Ru/C in 1.0 M PBS.

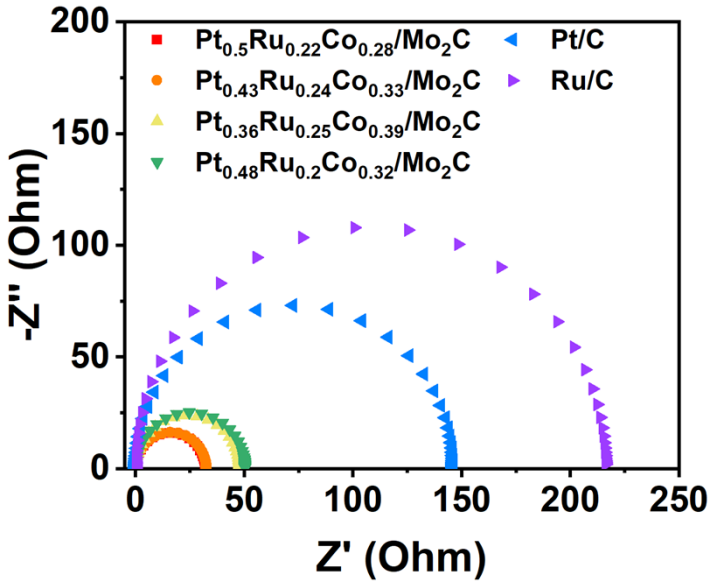

Figure S14. Nyquist plots of PtRuCo/Mo_2C series catalysts, Pt/C and Ru/C in 1.0 M PBS.

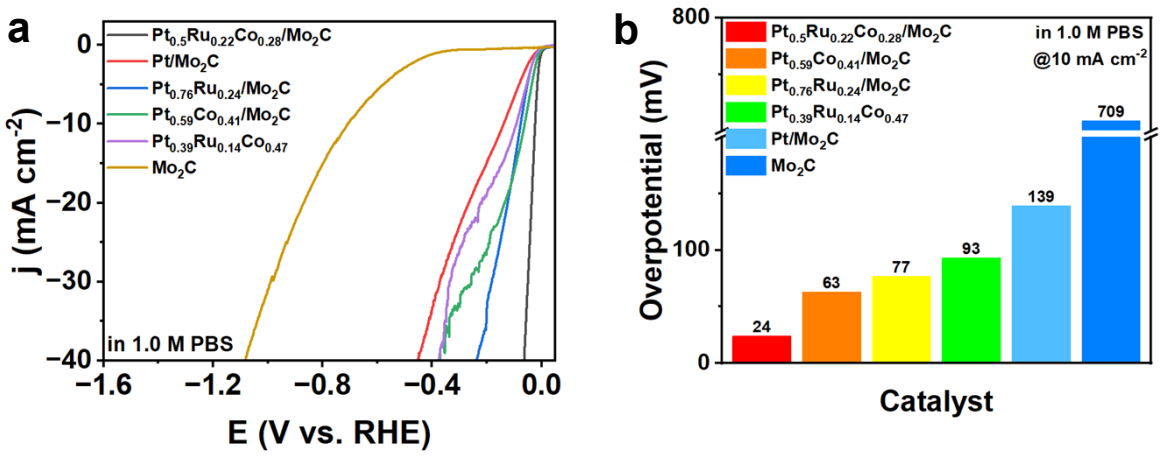

Figure S15. (a) LSV curves of $Pt_{0.39}Ru_{0.14}Co_{0.47}$, Pt/Mo_2C, $Pt_{0.76}Ru_{0.24}/Mo_2C$, $Pt_{0.59}Co_{0.41}/Mo_2C$, $Pt_{0.5}Ru_{0.22}Co_{0.28}/Mo_2C$ and Mo_2C in 1.0 M PBS and (b) overpotentials at 10 mA cm^{-2}.

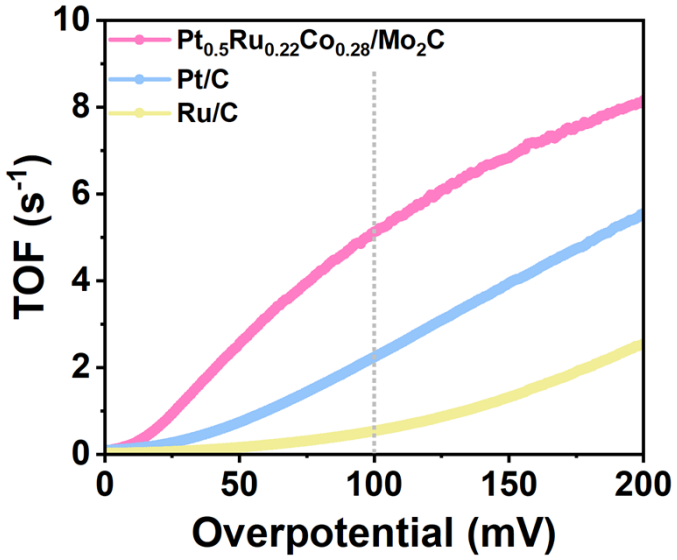

Figure S16. TOF values of $Pt_{0.5}Ru_{0.22}Co_{0.28}/Mo_2C$, Pt/C and Ru/C in 1.0 M PBS.

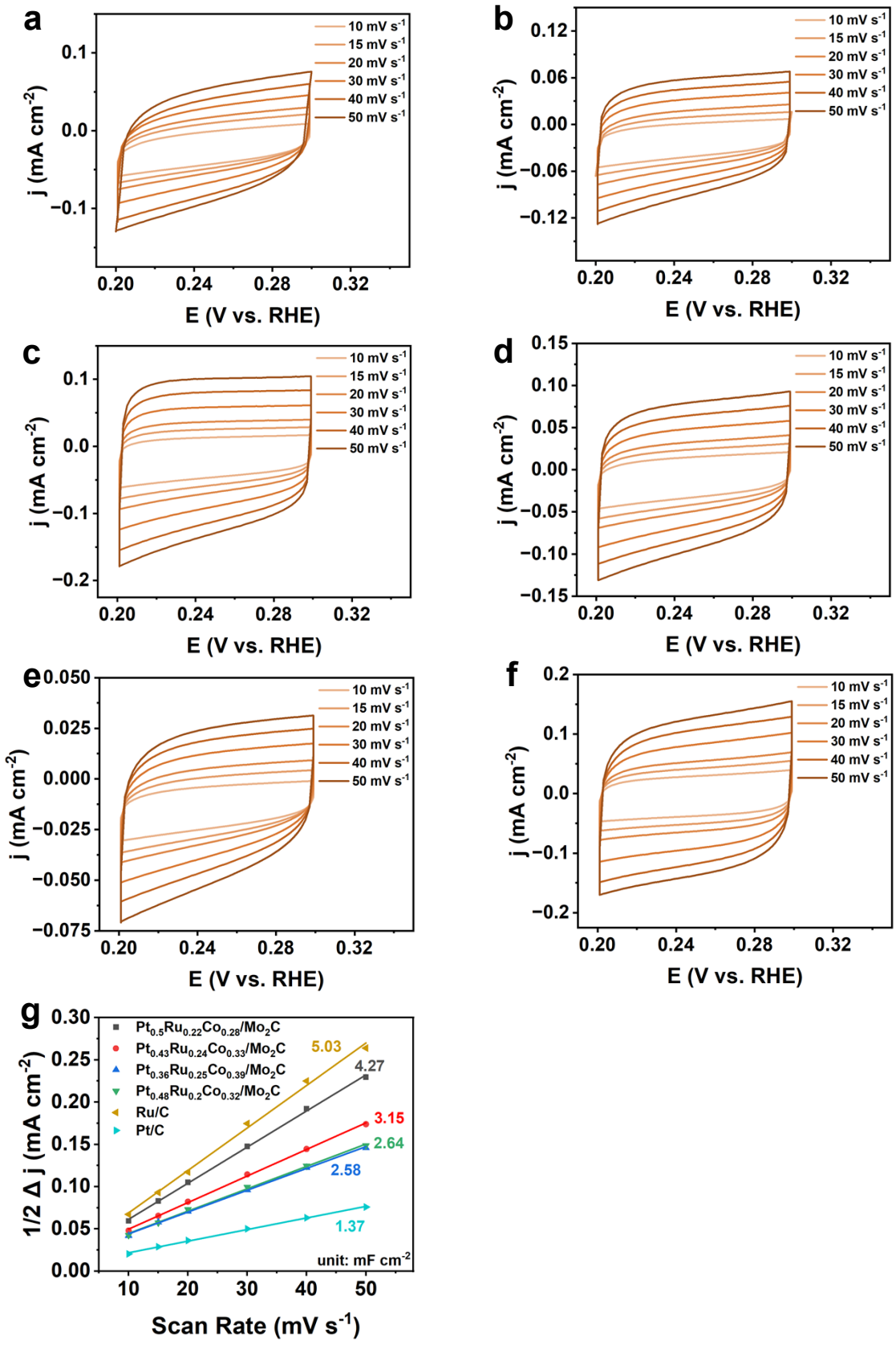

Figure S17. CV curves of the (a) $Pt_{0.36}Ru_{0.25}Co_{0.39}/Mo_2C$, (b) $Pt_{0.48}Ru_{0.2}Co_{0.32}/Mo_2C$, (c) $Pt_{0.5}Ru_{0.22}Co_{0.28}/Mo_2C$, (d) $Pt_{0.43}Ru_{0.24}Co_{0.33}/Mo_2C$, (e) Pt/C and (f) Ru/C. (g) C_{dl} of (a)-(f) in 1.0 M PBS.

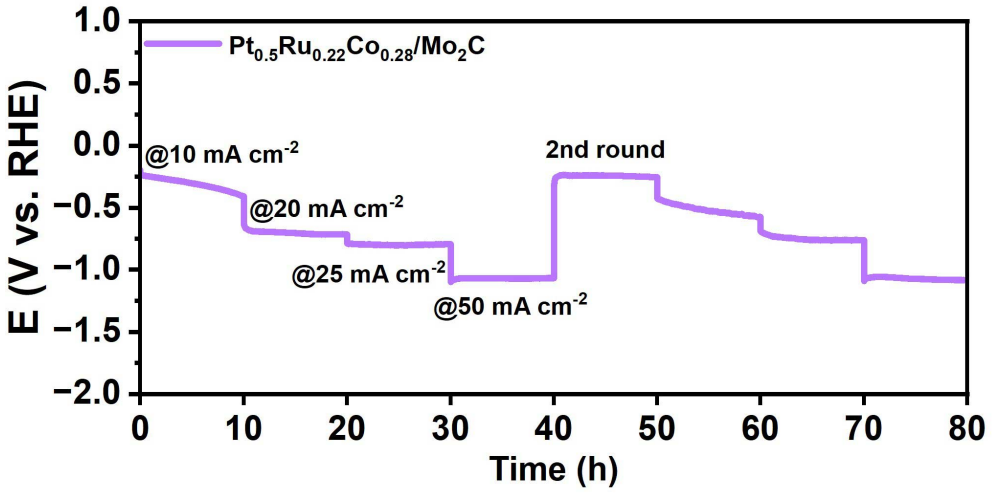

Figure S18. The Multi-Current Steps stability test of $Pt_{0.5}Ru_{0.22}Co_{0.28}/Mo_2C$ in 1.0 M PBS.

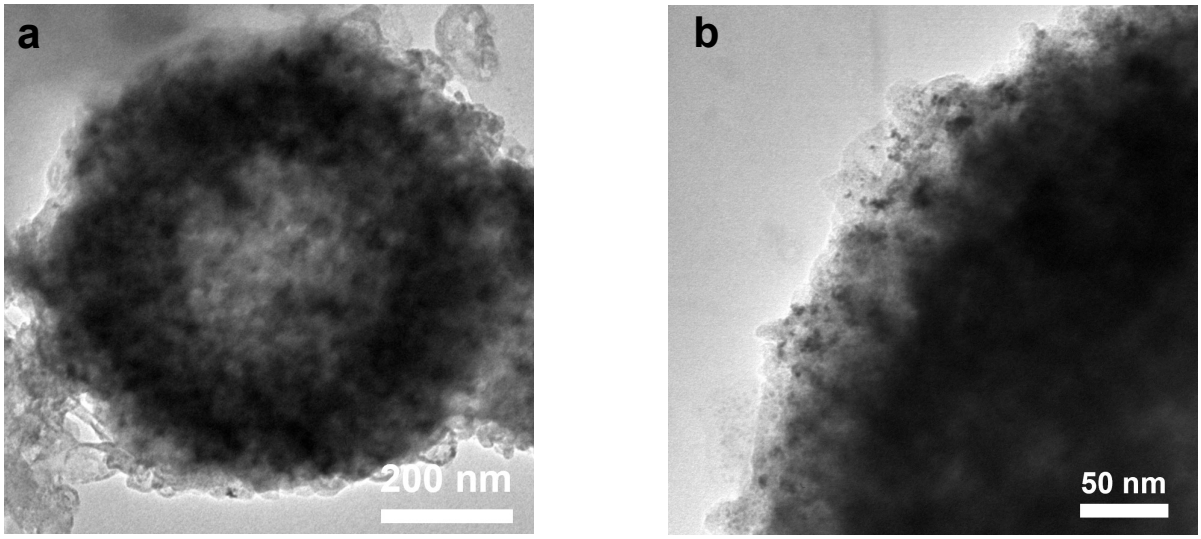

Figure S19. TEM images of $Pt_{0.5}Ru_{0.22}Co_{0.28}/Mo_2C$ after 70,000 CV cycles in 1.0 M PBS.

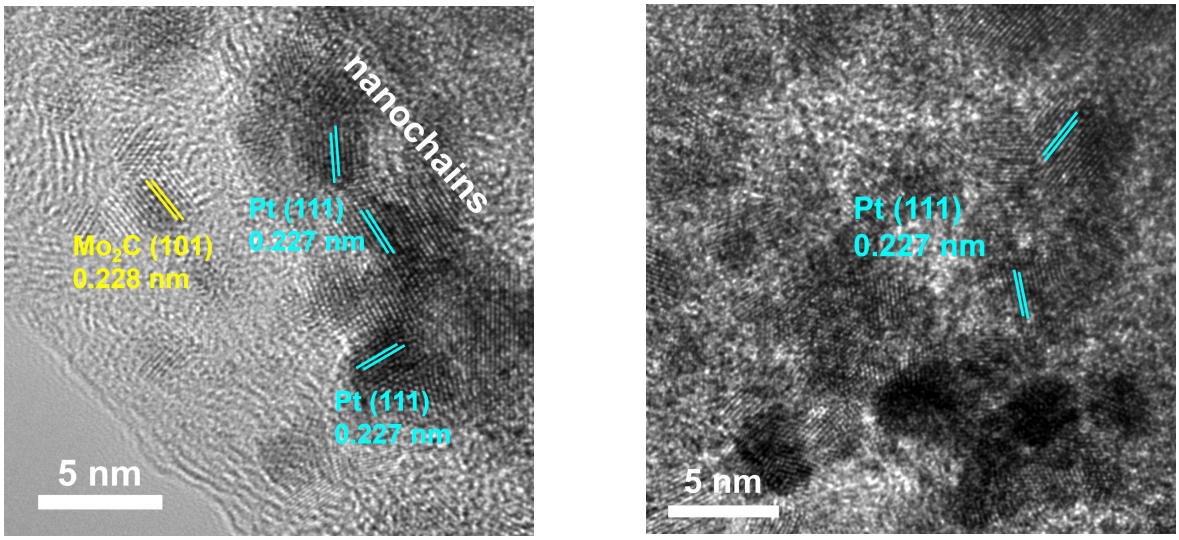

Figure S20. HRTEM images of $Pt_{0.5}Ru_{0.22}Co_{0.28}/Mo_2C$ after 70,000 CV cycles in 1.0 M PBS.

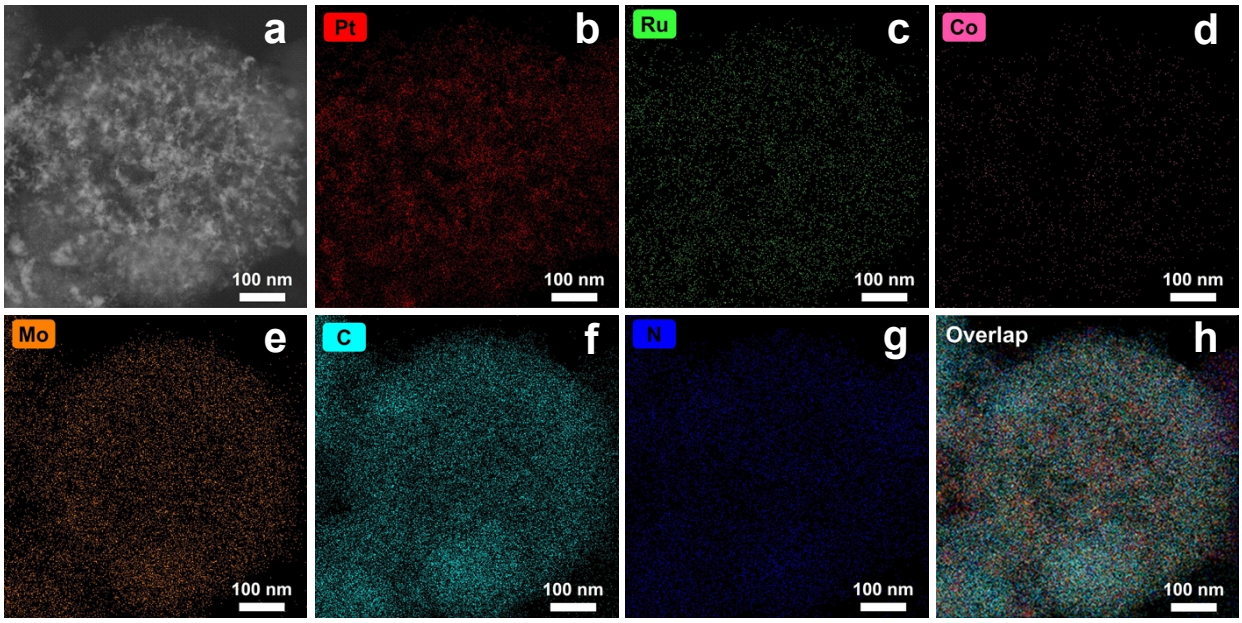

Figure S21. (a) STEM image, (b-h) corresponding EDS mapping and elemental overlap images of $Pt_{0.5}Ru_{0.22}Co_{0.28}/Mo_2C$ after 70,000 CV cycles in 1.0 M PBS.

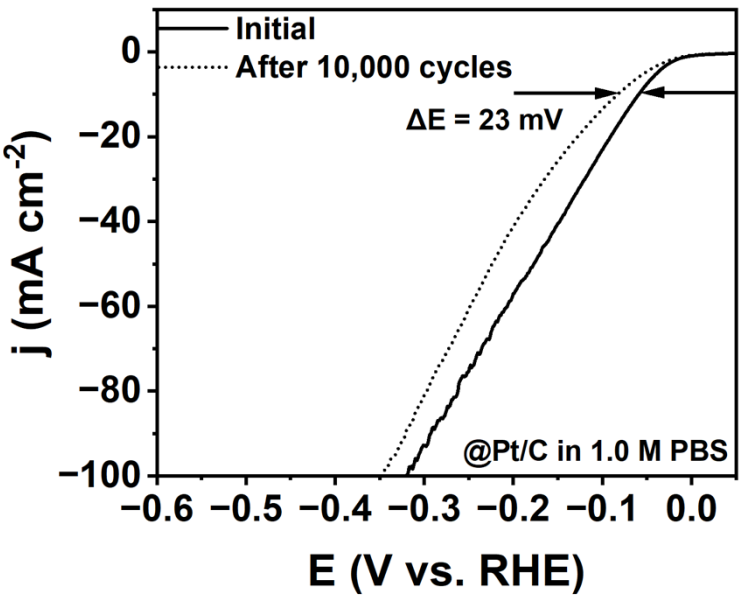

Figure S22. LSV curves before and after 10,000 cycles of Pt/C in 1 M PBS.

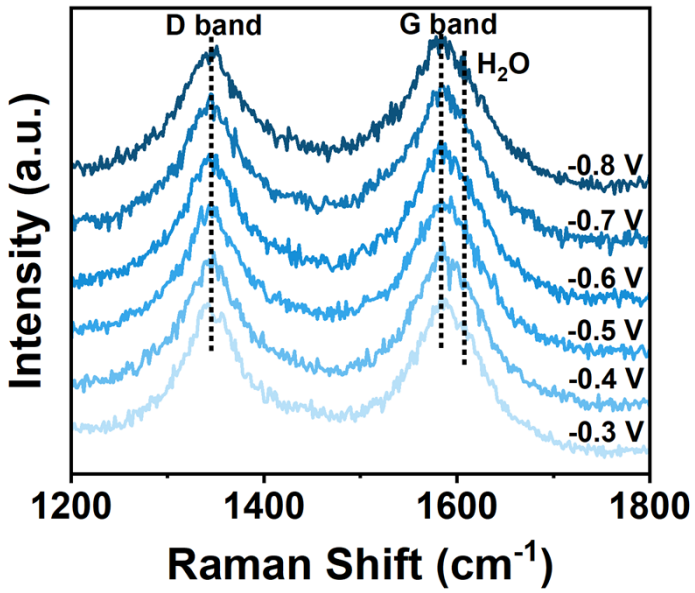

Figure S23. In-situ Raman spectrum of $Pt_{0.5}Ru_{0.22}Co_{0.28}/Mo_2C$ in 1.0 M PBS (a) 1200 cm^{-1}-1800 cm^{-1}.

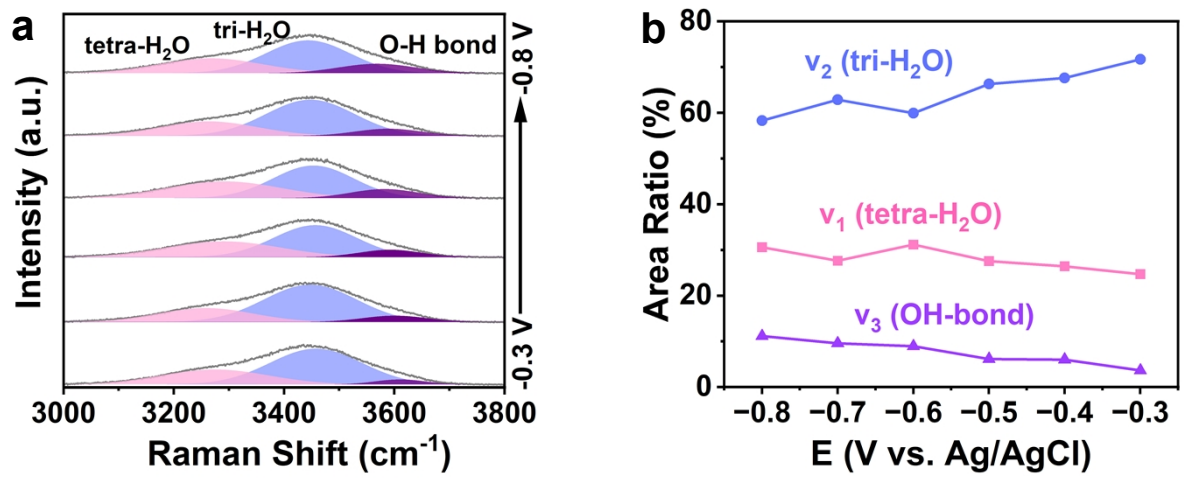

Figure S24. (a) In-situ Raman spectra of $Pt_{0.5}Ru_{0.22}Co_{0.28}/Mo_2C$ in 1.0 M PBS (a) 3000 cm^{-1}-3800 cm^{-1} and (b) The area ratio of different interfacial water modes.

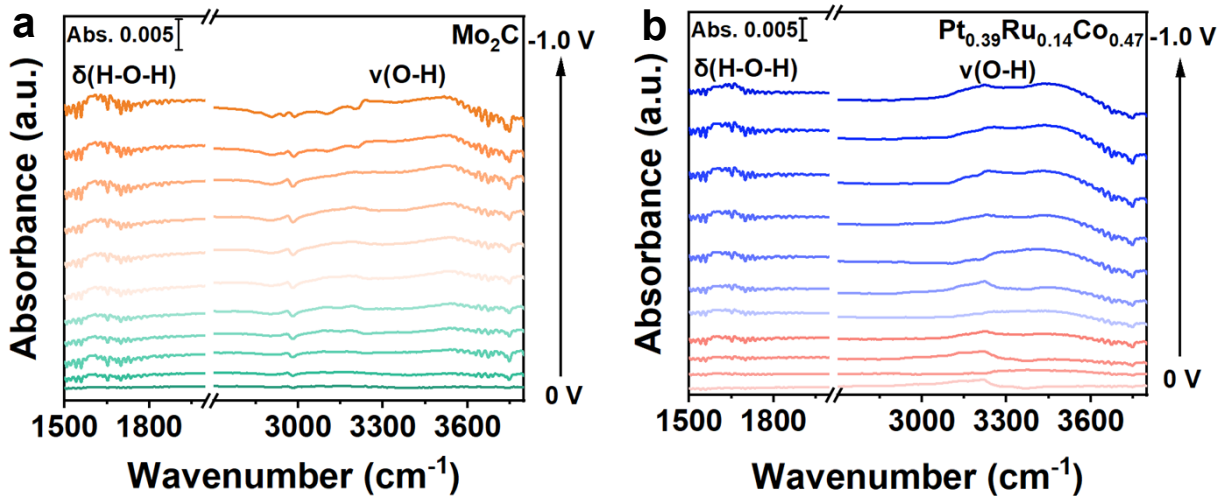

Figure S25. ATR-SEIRAS spectra of (a) $Pt_{0.39}Ru_{0.14}Co_{0.47}$, (b) Mo_2C.

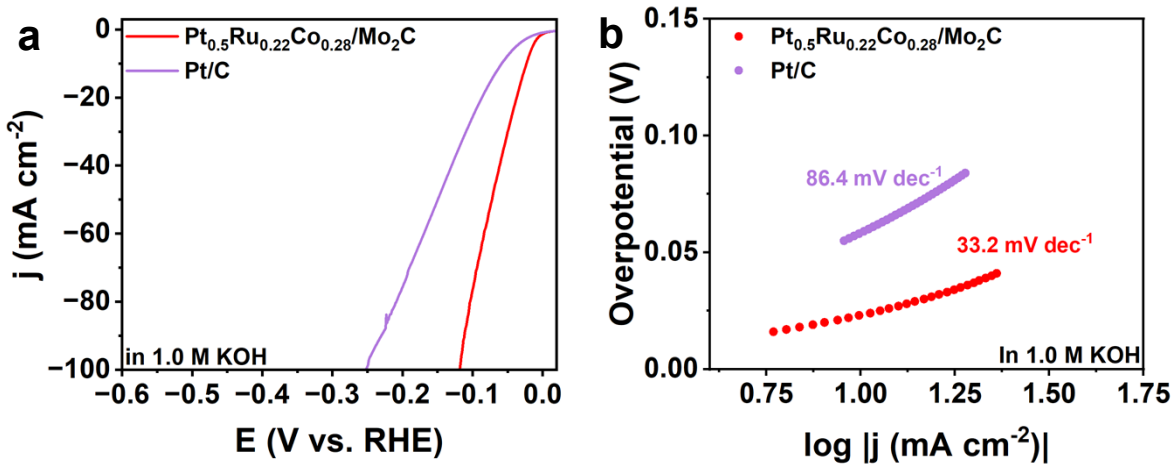

Figure S26. (a) HER performance of $Pt_{0.5}Ru_{0.22}Co_{0.28}/Mo_2C$ and Pt/C in 1.0 M KOH. (a) LSV curves and (b) corresponding Tafel slopes.

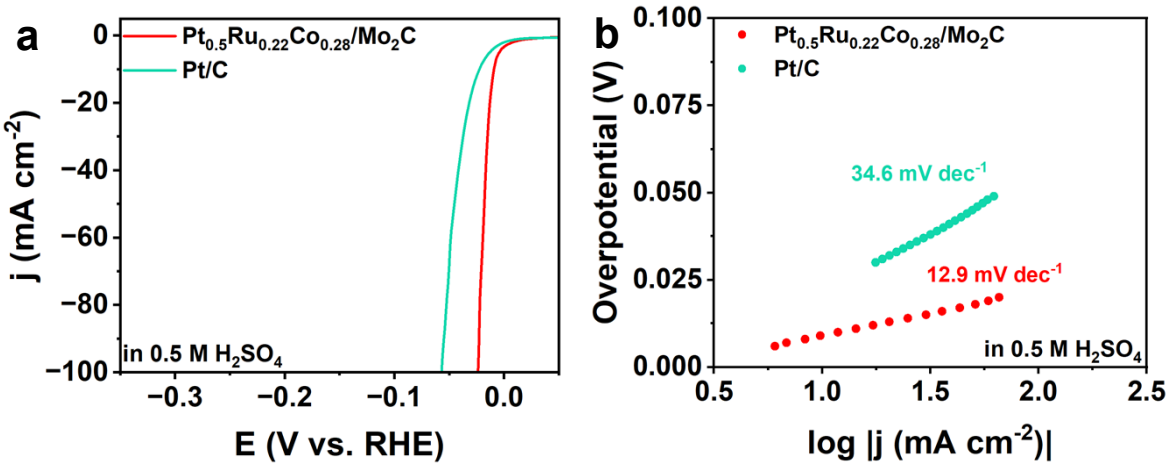

Figure S27. HER performance of $Pt_{0.5}Ru_{0.22}Co_{0.28}/Mo_2C$ and Pt/C in 0.5 M H_2SO_4. (a) LSV curves and (b) corresponding Tafel slopes.

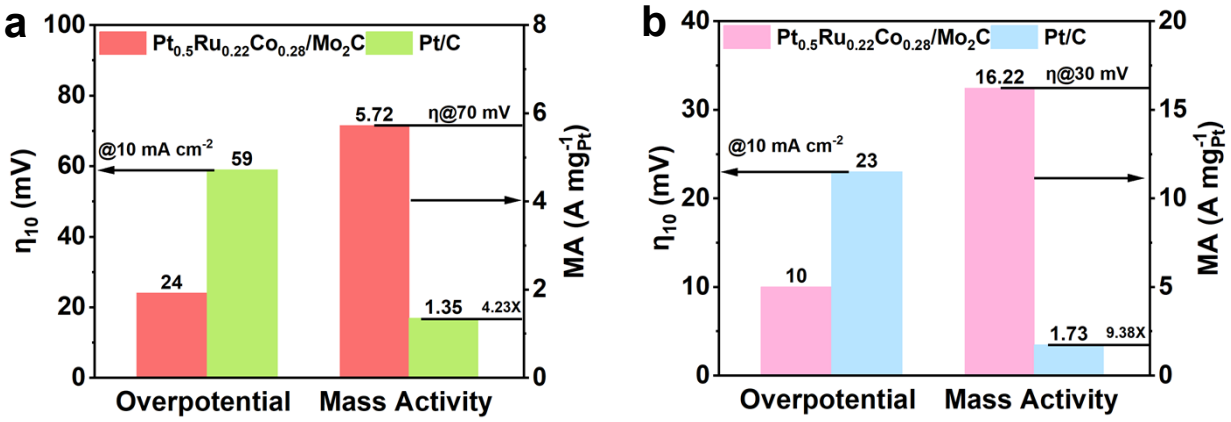

Figure S28. η_{10} and mass activity of $Pt_{0.5}Ru_{0.22}Co_{0.28}/Mo_2C$ and Pt/C in (a) 1.0 M KOH and (b) 0.5 M H_2SO_4.

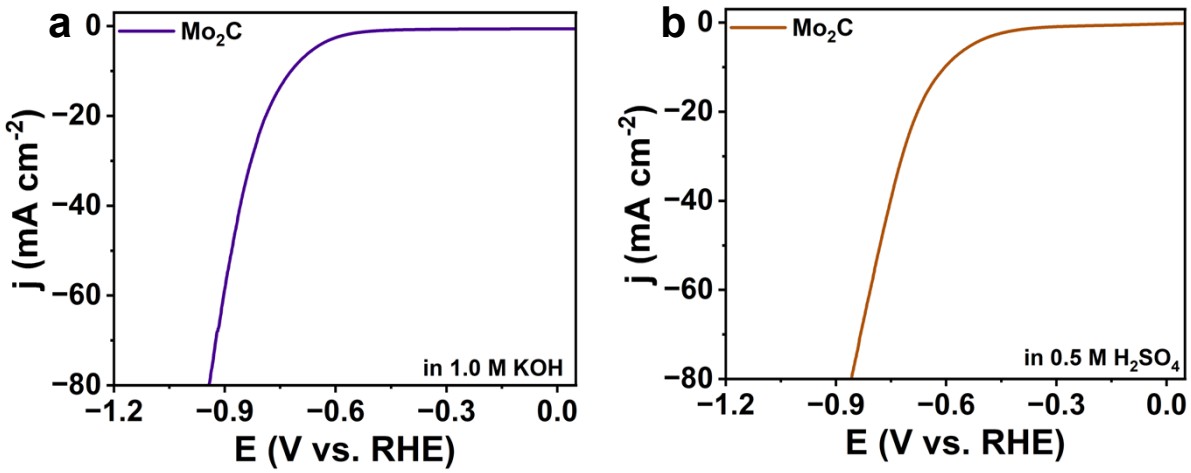

Figure S29. LSV curves for Mo_2C in (a) 1.0 M KOH and (b) 0.5 M H_2SO_4.

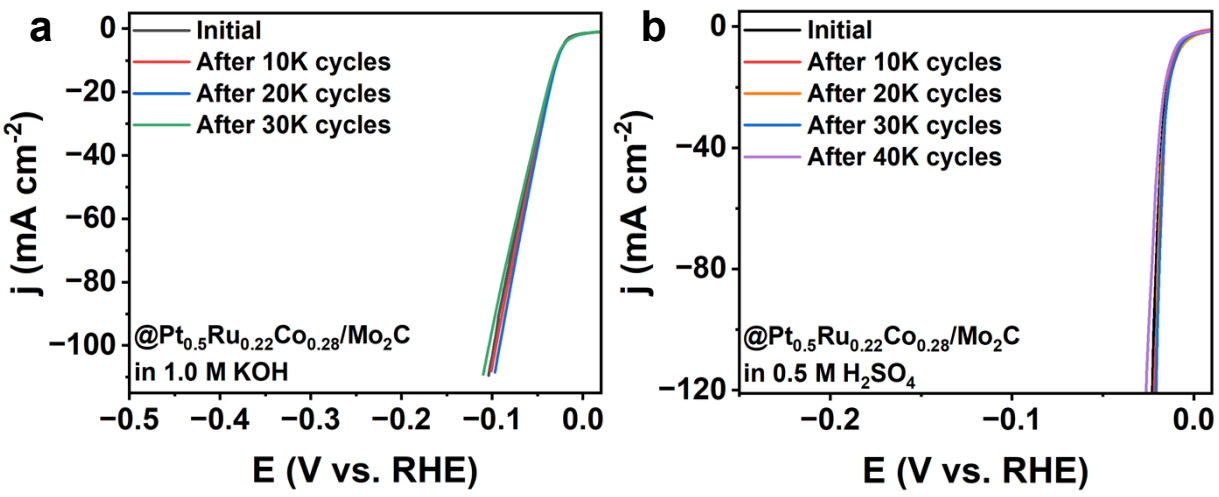

Figure S30. LSV curves for $Pt_{0.5}Ru_{0.22}Co_{0.28}/Mo_2C$ before and after CV cycles in (a) 1.0 M KOH and (b) 0.5 M H_2SO_4.

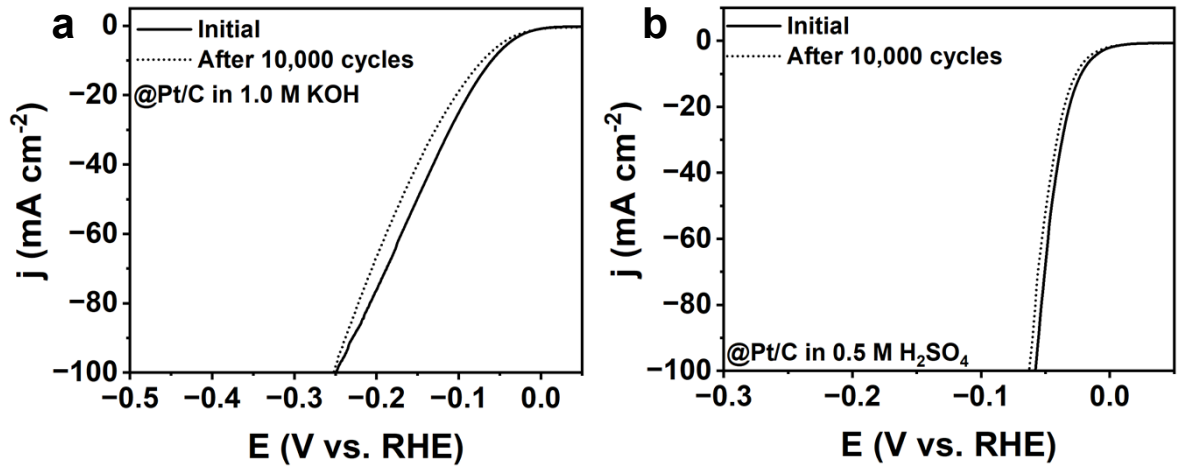

Figure S31. LSV curves before and after 10,000 cycles of commercial Pt/C in (a) 1.0 M KOH and (b) 0.5 M H_2SO_4.

Table S1. The ICP-OES results from different samples.

Samples	Pt (At %)	Ru (At %)	Co (At %)
$Pt_{0.5}Ru_{0.22}Co_{0.28}/Mo_2C$	50	22	28
$Pt_{0.43}Ru_{0.24}Co_{0.33}/Mo_2C$	43	24	33
$Pt_{0.36}Ru_{0.25}Co_{0.39}/Mo_2C$	36	25	39
$Pt_{0.48}Ru_{0.2}Co_{0.32}/Mo_2C$	48	20	32
Pt/Mo_2C	100	-	-
$Pt_{0.76}Ru_{0.24}/Mo_2C$	76	24	-
$Pt_{0.59}Co_{0.41}/Mo_2C$	59	-	41
$Pt_{0.39}Ru_{0.14}Co_{0.47}$	39	14	47

Table S2. Comparison of the HER performance between $Pt_{0.5}Ru_{0.22}Co_{0.28}/Mo_2C$ and other state-of-the-art electrocatalysts in 1.0 M PBS solution.

Catalysts	Overpotential @ η_{10} (mV)	Tafel slope (mV dec^{-1})	References
$Pt@CoO_x$	82	51.5	3
T-Pt-Co_4N	27	28.6	4
Pt_3Fe/NMCS-A	48	58	5
Pt-CoP	26.3	-	6
$Pt_{80}B_{20}$/C	47	49	7
Pt-NPO	33	33.3	8
HPMG-4	54	129	9
$PtCu_2$/CuO	47	49.5	10
Pt_3Ni/PC-700	61	66	11
MoN-5%Pt	62.9	65	12
Pt_{SA}/α-MoC_{1-x}/C	36	31	13
$Pt_{0.5}Ru_{0.22}Co_{0.28}/Mo_2C$	24	38.1	**This work**

Table S3. Comparison of recently reported high-performance advanced electrocatalysts for HER in 1.0 M PBS solution.

Catalysts	Stability	References
$PtCoW@CeO_2$	Stable for 50,000 cycles	14
Ru_1Pt_2@rGO	Stable for 3,000 cycles	15
Pt NPs@CF	Stable for 10,000 cycles	16
$Pt_{0.83}Ru_{0.17}/Mo_2C$	Stable for 5,000 cycles	17
Pt/CNT45	Stable for 2,000 cycles	18
MI-PtZnCo	Stable for 10,000 cycles	19
PtPdRhRuCu	Stable for 10,000 cycles	20
Pt_{SA}-Pt_c/NDPCM	Stable for 10,000 cycles	21
Pt@Cu-0.3	Stable for 1,000 cycles	22
PtRu/mCNTs	Stable for 3,000 cycles	23
$Pt_{0.63}Ru_{0.37}/PMo_{12}$	Stable for 20,000 cycles	24
$Pt_{0.5}Ru_{0.22}Co_{0.28}/Mo_2C$	Stable for 70,000 cycles	**This work**

Table S4. Comparison of the HER performance between $Pt_{0.5}Ru_{0.22}Co_{0.28}/Mo_2C$ and other state-of-the-art electrocatalysts in 1.0 M KOH solution.

Catalysts	Overpotential @ η_{10} (mV)	Tafel slope (mV dec^{-1})	References
Pt-MXene-12.5	32.8	32.8	25
Pt-Ru/ZrO_2	33	30	26
SA Pt-Ti_3C_2	59	36	27
PtCoCuNiZn	32.8	46	28
Pt_{SA}-Ni_2P@NF	26	34.1	29
np/Pt_1Ru_1-$Ni_{0.85}Se$	46	32.4	30
Pt_1/CeO_x	37	34	31
Pt/C60-2/KB	25	55	32
15% CoNiPt NFs	25	43	33
Ru@$Ru_{0.2}Rh_{0.2}Pd_{0.2}Pt_{0.2}Ir_{0.2\text{-}4L}$	50.8	63.7	34
PtRuMoZrRb HEA NPs	24	26	35
$Pt_{0.5}Ru_{0.22}Co_{0.28}/Mo_2C$	24	33.2	**This work**

Table S5. Comparison of the HER performance between $Pt_{0.5}Ru_{0.22}Co_{0.28}/Mo_2C$ and other state-of-the-art electrocatalysts in 0.5 M H_2SO_4 solution.

Catalysts	Overpotential @ η_{10} (mV)	Tafel slope (mV dec^{-1})	References
15 wt % Pt@3R-IrO_2	19	20.1	36
$Ti_3C_2T_x$-Pt_{SA}	38	45	37
3%Fe-PtSn/ATO	10.5	21	38
Pt/HE-LDH	42	42	39
1T-PtO_2	12	18.6	40
Pt–Er/h-NC	25	17.1	41
Pt/α-MoC	22	22	42
Pt NC@CPF-Fe	25	44.3	43
Pt@PtIr NDs	22	14.6	44
PtRuRhPdAuIr	16	40	45
Pt_3Sb	71	27	46
$Pt_{0.5}Ru_{0.22}Co_{0.28}/Mo_2C$	10	12.9	**This work**

References

[1] A. Salah, H.-D. Ren, N. Al-Ansi, F.-Y. Yu, Z. L. Lang, H. Tan and Y.-G. Li, *J. Mater. Chem. A*, 2021, **9**, 20518-20529.

[2] B. Zhou, J. Wang, L. Guo, H. Li, W. Xiao, G. Xu, D. Chen, C. Li, Y. Du, H. Ding, Y. Zhang, Z. Wu and L. Wang, *Adv. Energy Mater.*, 2024, **14**, 2402372.

[3] L. Zhai, X. She, L. Zhuang, Y. Li, R. Ding, X. Guo, Y. Zhang, Y. Zhu, K. Xu, H. J. Fan and S. P. Lau, *Angew. Chem. Int. Ed.*, 2022, **61**, e202116057.

[4] Z. Wu, Y. Zhao, W. Xiao, Y. Fu, B. Jia, T. Ma and L. Wang, *ACS Nano*, 2022, **16**, 18038-18047.

[5] P. Kuang, Z. Ni, B. Zhu, Y. Lin and J. Yu, *Adv. Mater.*, 2023, **35**, 2303030.

[6] H. Lei, Y. Zhou, Z. Huangfu, L. Chen, J. Cao, X. Yang, W. Mai and Z. Wang, *Adv. Sci.*, 2025, **12**, 2504462.

[7] H. Jiang, Y. Xiao, Z. Liu, Z. Wang, B. Wei, Q. Wei and N. Cheng, *J. Colloid Interface Sci.* 2025, **684**, 95-104.

[8] D. Wang, Y. Chen, B. Yao, T. Meng, Y. Xu, D. Jiao, Z. Xing and X. Yang, *J. Energy Chem.*, 2025, **101**, 808-815.

[9] X. Zhao, J. Liu, H. Zhang, J. Jiang, J. Lin, J. Fu, Y. Zhang, X. Li, W. Ruan and J. Ma, *Chem. Eng. J.*, 2025, **515**, 163667.

[10] M. Jiang, J. Xu, Q. Zhou, Y. Chen, P. Munroe, L. Li, Z.-H. Xie, Y. Wu and S. Peng, *Angew. Chem. Int. Ed.*, 2025, **64**, e202510259.

[11] G. Yang, L. Li, S. Cui, S. Han, Z. Xue, A. Wang and G. Wang, *Chem. Eng. J.*, 2025, **518**, 164842.

[12] V.-H. Do, Y. Li, P. Prabhu, W. Xie, P. Kidkhunthod, H. Wang, G. Wang and J.-M. Lee, *Adv. Funct. Mater.*, 2023, **33**, 2302297.

[13] W. Wang, Y. Wu, Y. Lin, J. Yao, X. Wu, C. Wu, X. Zuo, Q. Yang, B. Ge, L. Yang, G. Li, S. Chou, W. Li and Y. Jiang, *Adv. Funct. Mater.*, 2022, **32**, 2108464.

[14] J. Chen, T. Yu, Z. Zhai, G. Qian and S. Yin, *J. Energy Chem.*, 2023, **80**, 535-541.

[15] J. Yang, J. Feng, Y. Cao, Y, Xiao, L. Qiao, K, An, J. Yang, J. Peng, H. Pan and H.-M. Cheng, *Adv. Funct. Mater.*, 2024, **34**, 2411081.

[16] Q. Li, Z. Deng, D. Tao, J. Pan, W. Xu, Z. Zhang, H. Zhong, Y. Gao, Q. Shang, Y. Ni, X. Li, Y. Chen and Q. Zhang, *Adv. Funct. Mater.*, 2024, **34**, 2411283.

[17] H. Ling, Q. Yuan, T. Sheng and X. Wang, *J. Colloid Interface Sci.*, 2025, **685**, 371-381.

[18] Y. Liu, P. Liu, Y. Cai, M. Zhu, N. Dou, L. Zhang, Y.-L. Men and Y.-X. Pan, *Small*, 2025, **21**, 2411181.

[19] Y. Wang, H. Lv, L. Sun, F. Jia and B. Liu, *Adv. Energy Mater.*, 2022, **12**, 2201478.

[20] Y. Kang, O. Cretu, J. Kikkawa, K. Kimoto, H. Nara, A. S. Nugraha, H. Kawamoto, M. Eguchi, T. Liao, Z. Sun, T. Asahi and Y. Yamauchi, *Nat. Commun.*, 2023, **14**, 4182.

[21] W. Yang, M. Li, B. Zhang, Y. Liu, J. Zi, H. Xiao, X. Liu, J. Lin, H. Zhang, J. Chen, Z. Wan, Z. Li, G. Li, H. Li and Z. Lian, *Adv. Funct. Mater.*, 2023, **33**, 2304852.

[22] Y. Tan, R. Xie, S. Zhao, X. Lu, L. Liu, F. Zhao, C. Li, H. Jiang, G. Chai, D. J. L. Brett, P. R. Shearing, G. He and I. P. Parkin, *Adv. Funct. Mater.*, 2021, **31**, 2105579.

[23] B. Pang, X. Liu, T. Liu, T. Chen, X. Shen, W. Zhang, S. Wang, T. Liu, D. Liu, T. Ding, Z. Liao, Y. Li, C. Liang and T. Yao, *Energy Environ. Sci.*, 2022, **15**, 102-108.

[24] Y. Zhang, Y. Feng and Q. Yuan, *Int. J. Hydrogen Energy*, 2025, **162**, 150748.

[25] Z. Lei, S. Ali, C. I. Sathish, M. Ahmed, J. Qu, R. Zheng, S. Xi, X. Yu, M. B. H. Breese, C. Liu, J. Zhang, S. Qi, X. Guan, V. Perumalsamy, M. Fawaz, J.-H. Yang, M. Bououdina, K. Domen, A. Vinu, L. Qiao and J. Yi, *Nano-Micro Lett.*, 2025, **17**, 123.

[26] Q. Wang, Y. Chen, X. Zang, H. Li, W. Xiao, Y. Zong, G. Fu, J. Wang, Z. Wu and L. Wang, *Chem. Eng. J.*, 2025, **512**, 162421.

[27] T. Chu, G. Wang, X. Zhang, Y. Jia, S. Dai, X. Liu, L. Zhang, X. Yang, B. Zhang and F.-Z. Xuan, *Nano Lett.*, 2024, **24,** 9666-9674.

[28] H. Ren, Z. Zhang, Z. Geng, Z. Wang, F. Shen, X. Liang, Z. Cai, Y. Wang, D. Cheng, Y. Cao, X. Yang, M. Hu, X. Yao and K. Zhou, *Adv. Energy Mater.*, 2024, **14**, 2400777.

[29] D. Ren, G. Wang, L. Li, Y. Jin, K. Zhou, C. Zeng, Q. Zhang, J. Liu, R. Wang, X. Ke, M. Sui and H. Wang, *Chem. Eng. J.*, 2023, **454**, 140557.

[30] L. Cai, H. Bai, C.-w. Kao, K. Jiang, H. Pan, Y.-R. Lu and Y. Tan, *Small*, 2024, **20**, 2311178.

[31] V. Dao, G. Di Liberto, S. Yadav, P. Uthirakumar, K. Chen, G. Pacchioni and I.-H. Lee, *Nano Lett.*, 2024, **24**, 1261-1267.

[32] R. Zhang, Y. Li, X. Zhou, A. Yu, Q. Huang, T. Xu, L. Zhu, P. Peng, S. Song, L. Echegoyen and F.-F. Li, *Nat. Commun.*, 2023, **14**, 2460.

[33] Y. Pan, J. Gao, E. Lv, T. Li, H. Xu, L. Sun, A. Nairan and Q. Zhang, *Adv. Funct. Mater.*, 2023, **33**, 2303833.

[34] T.-H. Hu, C.-Y. Wu, Z. Y. He, Y. Chen, L.-C. Hsu, C.-W. Pao, J.-T. Lin, C.-W. Chang, S.-C. Lin, R. Osmundsen, L. Casalena, K. H. Lin, S. Zhou and T.-H. Yang, *Adv. Sci.*, 2024, **12**, 2409023.

[35] H. Zhuo, Q. Song, C. Wang and H. Zhu, *Chem. Commun.*, 2025, **61**, 11227-11230.

[36] R. Guo, J. Wang, J. Li, H. Li, H. Wang, Y. Cao, J. Chen, T. Cheng, H. Yang and M. Sheng, *ACS Catal.*, 2024, **14**, 11164-11171.

[37] J. Zhang, E. Wang, S. Cui, S. Yang, X. Zou and Y. Gong, *Nano Lett.*, 2022, **22**, 1398-405.

[38] Z. Zhang, W. Wu, S. Chen, Z. Wang, Y. Tan, W. Chen, F. Guo, R. Chen and N. Cheng, *Small*, 2024, **20**, 2307135.

[39] H. Xu, Y. Liu, K. Wang, L. Jin, J. Chen, H. Chen and G. He, *J. Colloid Interface Sci.*, 2025, **684**, 566-574.

[40] H. Yang, Y. Ji, Q. Shao, W. Zhu, M. Fang, M. Ma, F. Liao, H. Huang, Y. Zhang, J. Yang, Z. Fan, Y. Li, Y. Liu, M. Shao and Z. Kang, *Energy Environ. Sci.*, 2023, **16**, 574-583.

[41] G. Chen, W. Chen, R. Lu, C. Ma, Z. Zhang, Z. Huang, J. Weng, Z. Wang, Y. Han and W. Huang, *J. Am. Chem. Soc.*, 2023, **145**, 22069-22078.

[42] W. Liu, A. Wang, J. Zhang, S. Yu, M. Wang, S. Tian, H. Tang, Z. Zhao, X. Ren, Y. Guo and D. Ma, *ACS Nano*, 2025, **19**, 10038-10047.

[43] Z.-D. Wang, Y. Han, Y.-Y. Wang, S.-Q. Zang and P. Peng, *Angew. Chem. Int. Ed.*, 2025, **64**, e202416973

[44] C. Liu, Z. Wei, M. Cao and R. Cao, *Nano Res.*, 2024, **17**, 4844-4849.

[45] C. Chen, W. Wu, P. Chen, J. Guo, H. Bian, W. Li, X. Zhao and L. Wei, *Chem. Commun.*, 2025, **61**, 6787-6790.

[46] Y. Zhang, J. Si, Z. Chen, S. Hu, F. Qiu, W. Li, W. Zhang and S. Miao, *Nano Lett.*, 2025, **25**, 4416-4423.